

Original article:

Glioma segmentation with DWI weighted images, conventional anatomical images, and post-contrast enhancement magnetic resonance imaging images by U-Net

Amir Khorasani 1, Rahele Kafieh 2,4, Masih Saboori 3, Mohamad Bagher Tavakoli 1*

1. Department of Medical Physics, School of Medicine, Isfahan University of Medical Sciences, Isfahan, Iran.
2. Medical Image and Signal Processing Research Center, School of Advanced Technologies in Medicine, Isfahan University of Medical Sciences, Isfahan, Iran.
3. Department of Neurosurgery, School of Medicine, Isfahan University of Medical Sciences, Isfahan, Iran.
4. Department of Engineering, Durham University, Durham, UK

***Corresponding author:** M. B. Tavakoli

Department of Medical Physics, School of Medicine, Isfahan University of Medical Sciences, Isfahan,
Iran

Postal code: 81746-73461

Phone: +98-31-37929095

Fax: +98-31-36688597

E-mail: mbtavakoli@mui.ac.ir

Abstract

Glioma segmentation is believed to be one of the most important stages of treatment management. Recent developments in magnetic resonance imaging (MRI) protocols have led to a renewed interest in using automatic glioma segmentation with different MRI image weights. U-Net is a major area of interest within the field of automatic glioma segmentation. This paper examines the impact of different input MRI image-weight on the U-Net output performance for glioma segmentation. One hundred forty-nine glioma patients were scanned with a 1.5T MRI scanner. The main MRI image-weights acquired are diffusion-weighted imaging (DWI) weighted images (b50, b500, b1000, Apparent diffusion coefficient (ADC) map, Exponential apparent diffusion coefficient (eADC) map), anatomical image-weights (T₂, T₁, T₂-FLAIR), and post enhancement image-weights (T₁Gd). The U-Net and data augmentation are used to segment the glioma tumors. Having the Dice coefficient and accuracy enabled us to compare our results with the previous study. The first set of analyses examined the impact of epoch number on the accuracy of U-Net, and n_epoch=20 was selected for U-Net training. The mean Dice coefficient for b50, b500, b1000, ADC map, eADC map, T₂, T₁, T₂-FLAIR, and T₁Gd image weights for glioma segmentation with U-Net were calculated 0.892, 0.872, 0.752, 0.931, 0.944, 0.762, 0.721, 0.896, 0.694 respectively. This study has found that, DWI image-weights have a higher diagnostic value for glioma segmentation with U-Net in comparison with anatomical image-weights and post enhancement image-weights. The results of this investigation show that ADC and eADC maps have higher performance for glioma segmentation with U-Net.

Keywords: Glioma, Segmentation, Apparent diffusion coefficient, Exponential apparent diffusion coefficient, U-Net.

1. Introduction

The glioma is a brain or spine tumor originating from the glial cells [1]. Gliomas are involved in 80% of all malignant brain tumors [2]. Based on the tumor aggressiveness and growth potential, gliomas are classified into ‘low-grade’ and ‘high-grade’ [3]. Glioma segmentation and detection are essential processes for treatment decisions. With the development in medical imaging, there has been an increasing role of imaging technology in glioma diagnosis and detection [4]. Magnetic resonance imaging (MRI) is a powerful imaging technology within the field of glioma detection due to its soft tissue contrast, image resolution, non-invasive imaging, non-ionizing radiation imaging modality, and different imaging protocols and image-weights [5]. Glioma segmentation on the medical images plays an essential role in the treatment decision and provides important data such as tumor location, tumor size, the growth state, the change process of the tumor, and the follow-up of the brain tumor. So, the issue of accurate glioma segmentation has received considerable critical attention [6].

In the classical approach, glioma segmentation is based on radiologist’s observation and experience, leading to poor intra-observer difference, time-consuming process, and low diagnosis stability [7]. In recent years, there has been an increasing interest in computer-aided diagnosis and detection for glioma segmentation [7]–[11]. One of the most significant current automated manners in glioma classification is deep convolution neural network (DCNN) [9], [12], [13]. DCNN is a new method that has been shown to be effective in brain tumor classification and detection using large training data sets [14]. There is massive research on DCNN with different MRI image-weights for glioma segmentation [13], [15]–[20]. U-Net is one of the most widely DCNN architectures used for tumor segmentation and classification. In [21], the authors investigated U-Net usage for glioma segmentation with anatomical MRI image-weights (T1, T2, FLAIR) and post-contrast enhancement (T1Gd) protocols. It has been suggested [22] that the ADCmaps and automatic segmentation combination are valuable, and this seems to be an innovative approach for glioma segmentation. However, a major problem with this kind of application is, determining the proper MRI image-weight for the U-Net input image for tumor segmentation.

To increase the glioma segmentation accuracy and performance, we can use different network architectures to extract more information from data or use input images as training data with more information (images with physiological data instead of anatomical data) [23]–[27]. Many studies have been published on improving U-Net architecture for glioma segmentation [23]–[26]. One of the significant drawbacks to using this method is the time-consuming, high cost for the PC hardware process. In the light of the recent improvement in MRI imaging protocols and introduce MRI image-weights in which image contrast is based on physiological data, there is now some solution for improving glioma segmentation performance with the conventional U-Net architecture and the use of MRI image-weights with physiological data as data sets for U-Net training.

Most studies in the glioma segmentation with U-Net have only focused on using anatomical MRI image-weights as image data sets for U-Net training. Several attempts have been made to glioma segmentation by U-Net network with BraTs data set, which consist of T₁, FLAIR, and T₁ post enhancement (T₁Gd) MRI image-weights [28]–[32]. Image contrast on T₁, T₂, and inversion-

recovery sequences such as FLAIR, which are used in BraTs data sets, are based mainly on anatomical data [33]. One way to overcome these problems is to use different MRI image-weights with different information for glioma segmentation. Diffusion of water molecules is a fundamental property of diffusion-weighted imaging (DWI) image [34], and DWI image contrast is based on different tissue diffusion of water molecules [35]. There is a large volume of published studies describing the important role of DWI in neuroimaging and glioma studies [36]–[38].

This research examines the role of DWI image-weights as conventional U-Net architecture input images in glioma segmentation and compares the U-Net performance results with anatomical image weights. The primary objective of this study was to investigate which DWI weighted images (b50, b500, b1000, Apparent diffusion coefficient (ADC) map, Exponential apparent diffusion coefficient (eADC) map), anatomical image-weights (T_2 , T_1 , T_2 -FLAIR), and post enhancement image-weights (T_1 Gd), are appropriate and have high diagnostic value as training and test input MRI image-weights for glioma segmentation with conventional U-Net. In this context, we tried to introduce the best training and test input MRI image-weights used in this study for glioma segmentation by conventional U-Net architecture. There are several important areas where this study makes an original contribution to the importance of MRI physiological image-weights, such as DWI in conventional and original U-Net architecture training for glioma segmentation. Instead of U-Net architecture and anatomical images in this work, we focus on using DWI (b50, b500, b1000, ADC map, eADC map) as U-Net image inputs to improve the glioma segmentation performance.

2. Material and methods

The main stages of this research are shown in Figure 1. Before undertaking the investigation, ethical clearance was obtained from all of the patients. After collection, the patients were scanned with MRI, and required imaging sequences were obtained. Following this, image preprocessing (denoising, normalization, and resizing) was conducted to improve the input image quality for U-Net training. After the image preprocessing, it was necessary to create the mask of each tumor image in all MRI image-weights. In the next stage, training and evaluation of the U-Net with model specification and parameters were carried out. In the end, results were collected and compared with each other.

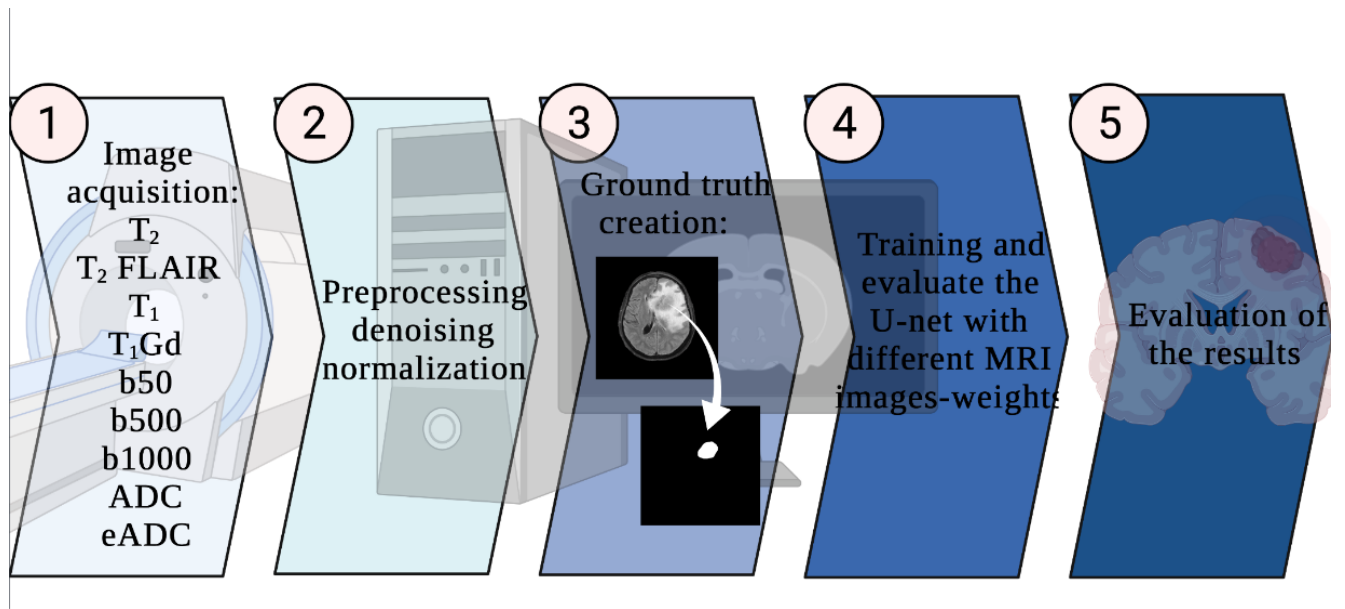


Figure 1- Main stage of the current study. This study is made of 5 different stages. 1-different MRI image weights acquisition. 2- preprocessing 3-mask and mask creation. 4- U-Net training phase. 5- data evaluation.

2.1. Patients

Patients were included in the study with the following inclusion criteria:

- 1- Histopathology confirmation of the glioma.
- 2- No radiation therapy or chemotherapy was performed before the MRI exam.
- 3- Sufficient image quality without patient motion and MRI artifacts.
- 4- No claustrophobia to the MRI.
- 5- Do not have an allergy to the gadolinium-based contrast agent.

Totally 149 patients were included in the current study. Before the MRI exam, all patients provided informed consent, and the local research ethics committee of Isfahan University of medical sciences, Isfahan, Iran, approved the study (ID: IR.MUI.MED.REC.1399.252).

2.2. MRI scanning

All patients were scanned at a 1.5T MRI scanner (GE MRI signal explorer 1.5T). We performed the following sequences: a 3-plane localizer sequence, Axial DWI weighted images (b50, b500, b1000, ADC map, eADC map), Axial T₂ weighted images, Axial T₁ weighted images, Axial T₁ post-contrast enhancement (T₁Gd) weighted images, and Axial T₂-Fluid-attenuated inversion recovery (FLAIR) weighted images pulse sequences. The pulse sequence parameters are listed in table 1. ADC and eADC maps were reconstructed with GE MRI WorkStation for each patient

$[ADC = \log(S_1/S_2)/(b_2 - b_1)]$; S_1 and S_2 : signal intensity of DWI images with two different b-Values (b_2 and b_1). After image acquisition and mask definition by experts, the patient images and masks were transferred to the personal computer (PC).

Table 1- Magnetic resonance imaging scanning parameters. Abbreviations: TR; time of repetition. TE; time of echo. FOV; field of view. DWI; Diffusion-weighted imaging. ADC; apparent diffusion coefficient. eADC; Exponential apparent diffusion coefficient. FLAIR; fluid attenuation inversion recovery.

Image weights	TR (ms)	TE (ms)	FOV (mm)	b-value (s/mm²)	Matrix size	Thickness (mm)	Gap (mm)
DWI	5268	113.2	240×240	50	512×512	5	5
DWI	5268	113.2	240×240	500	512×512	5	5
DWI	5268	113.2	240×240	1000	512×512	5	5
ADC	5211	110	240×240	50-1000	512×512	5	5
eADC	5211	110	240×240	50-1000	512×512	5	5
T₂	4134	109.4	240×240	-	512×512	5	5
T₂-FLAIR	8500	97.05	240×240	-	512×512	5	5
T₁	400	10	240×240	-	512×512	5	5
T₁Gd	6.1	2.2	240×240	-	512×512	5	5

2.3. Preprocessing

Image intensity values can change due to not only by different tissue types but also can change due to noise and scanner artifacts. It has been suggested [39] that intensity normalization has a significant role as a preprocessing stage. The purpose of intensity normalization is to uniformized the mean and variance values of image intensities. We used the normalization process to enable us to change the range of pixel intensity values in ranges 0 and 1. More details for normalization are given in [40]. We used simple noise reduction and image smoothing for all images to improve the U-Net input image quality. The denoising, normalization, and resizing processes were run using custom code written in the OpenCV-Python library. Also, all image sizes were changed to 256×256 to reduce the U-Net training time according to our GPU computational capability and memory (NVIDIA GeForce GTX-1060 with 6 GB memory).

2.4. Manual segmentation for mask creation

All masks for the U-Net training phase were created by two neuro-radiologists with 15 years of experience in glioma diagnosis independently. The software program used for mask creation was ImageJ. Radiologists manually specified the tumor boundaries enhancement at each image slice in T1Gd images for each patient using corresponding T1, T2, and T2-FLAIR MRI image-weights. The necrotic regions, edema regions, hemorrhage, and artifacts, if the tumor included, were avoided if possible. After determining the border of the tumor, the tumor border was drawn and copied to all other MRI image weights (T1, T2, T2-FLAIR, b50, b500, b1000, ADC map, eADC map) for each image slice. Finally, the mask of all MRI image weights was created and used for U-Net training and testing.

2.5. Data augmentation

For the effective training of various deep learning models, abundant and high-quality data is essential [41], [42]. A significant problem with collecting enough high-quality image data sets, especially for the medical domain, is time-consuming, expensive, and nearly impossible in practice. The data augmentation technique was done to overcome this limitation and lacks a satisfactory amount of data as an input image of deep learning models. As Goceri [42] mentioned, image augmentation has been widely used to overcome the data shortage problem in Deep-Learning based methods in medicine.

Data augmentation techniques can generally be divided into geometric transformation and artificial data generation. The geometric transformation technique is a major area of interest in data augmentation for deep learning because of the simplicity of the process. The data augmentation technique was performed using Keras ImageDataGenerator. **ImageDataGenerator provides an easy, quick, and real-time way to augment our data with very different augmentation techniques.** For data augmentation purpose and increasing the deep learning model's generalization capabilities, we employ most useable data augmentation techniques such as rotation, skewness, flipping, and shear to increase the training data effectively (rotation_range=0.2, width_shift_range=0.05, height_shift_range=0.05, shear_range=0.05, zoom_range=0.05).

2.6. U-Net training

This study used U-Net for medical image segmentation with different MRI image-weights as the input image. For this purpose, we designed and used a U-Net, which the details and architecture are given in Figure 2. U-Net architecture in the current study consists of 19 convolution layers with kernel size 3×3 with ReLU activation function, and same padding and kernel_initializer='he_normal', four max-pooling layers with kernel size 2×2 , four up-convolution (up-sampling) layers with kernel size 2×2 , four concatenate layers one convolution layers with kernel size 1×1 with Sigmoid activation function in the last layer. The number of filters and image size in each layer of U-Net, which we used, can be found in figure 2. U-Net compiles operation was performed by 'binary cross-entropy' loss function, 'Adam' optimizer, and 'accuracy' as metrics.

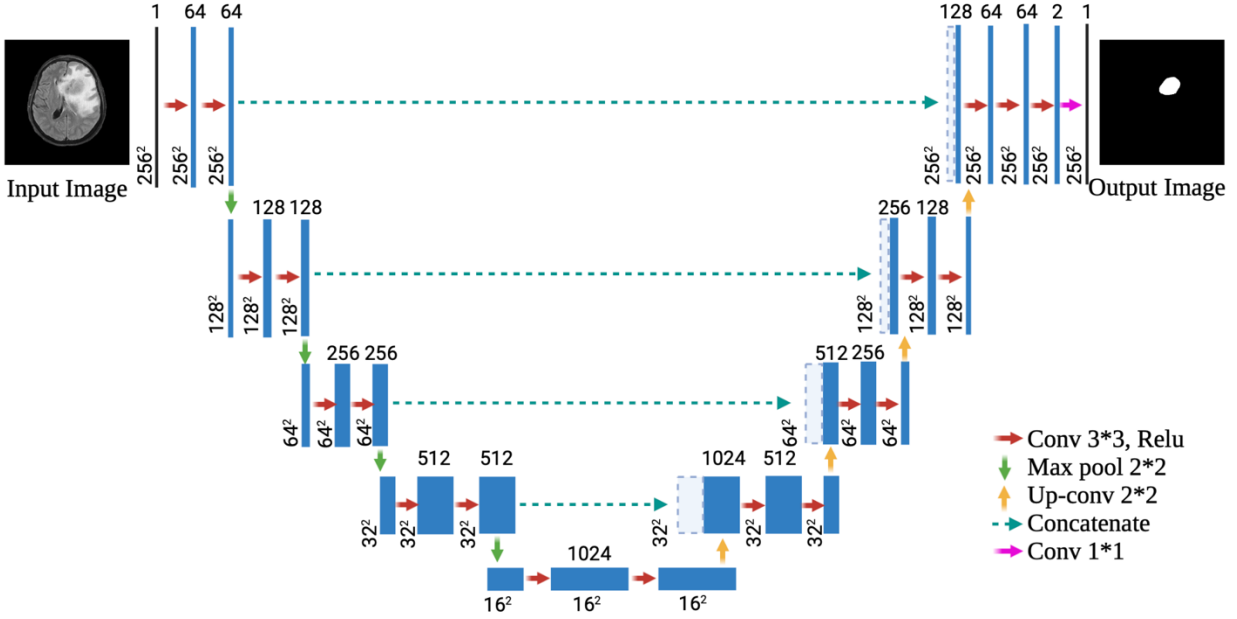


Figure 2- U-Net architecture and parameters which were used in this study. Each box with the number of channels above corresponds to a multi-channel feature map. The feature map size is shown on the lower side of the box. The arrows with different colors represent different operations.

The total number of parameters in our U-Net is 31,031,685, and all are trainable. The U-Net architecture was designed with TensorFlow (TensorFlow-GPU version 2.1.0) and Keras (version 2.3.1) on the Python (version 3.6) platform.

To find the correct epoch numbers for training the U-Net, we run U-Net with different epochs and calculated the accuracy of the network. We used the validation split=0.2 during the training phase to create the validation data sets from the training data set.

2.7. Performance evaluation methods of U-Net

Accuracy [14], [43], [44] (ACC, equation 1) is a metric that generally describes how the model performs. It is calculated as the ratio between the number of correct predictions to the total number of predictions.

$$ACC = \frac{TP + TN}{TP + TN + FP + FN} \quad \text{equation 1}$$

Where TP is true positive, TN is true negative, FP is false positive, and FN is false negative. TP gives all tumor regions, TN represents all non-tumoral regions, FN shows tumor regions that U-Net does not classify, and FN describes tumor region that is wrongly classified as tumor region. By using the 'validation split' function during the U-Net training phase, and 'accuracy' metrics, the ACC of U-net on validation data sets can be calculated.

The Dice coefficient (equation 2) [14], [44], [45] is used to measure the similarity between two sets of data.

$$Dice = \frac{2 \times (P \cap M)}{(|P| + |M|)} \quad \text{equation 2}$$

Where P represents the U-Net prediction and M represents the mask. After the trained U-Net made its prediction on test data sets, average Dice coefficients were calculated on different test data sets.

3. Results

To evaluate the effect of the number of epochs for the training process on accuracy and choice of the optimal number of epochs, figure 3 was used. As shown in figure 3, the results indicated that we had chosen epoch=20 for the U-Net training. Accuracy from epoch 1 to 20 rises quickly, reaches the optimal value at 20 epochs, and increases very slowly. The U-Net trained after 20 epochs were used in this study for the testing process.

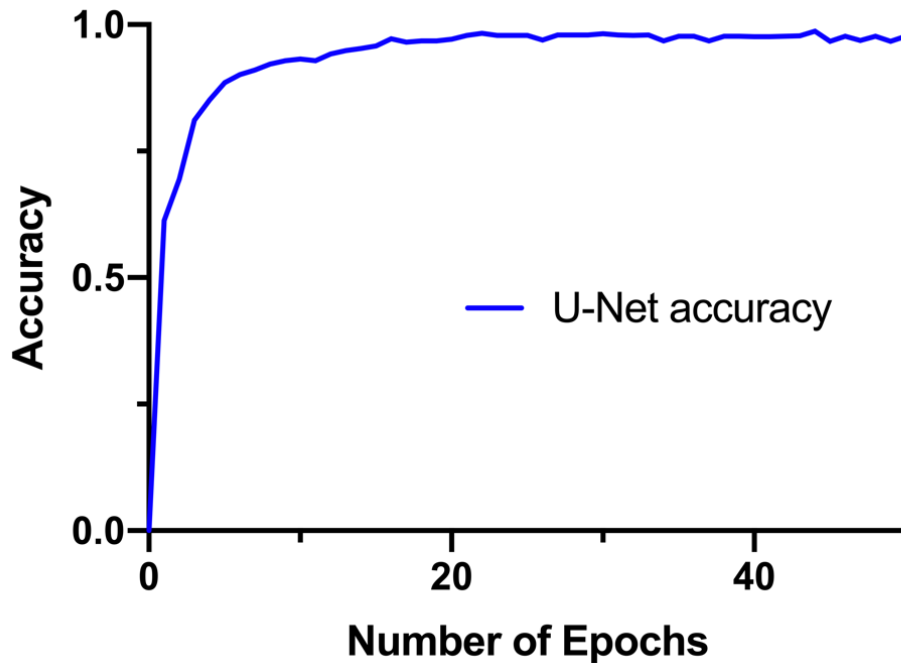


Figure 3- Training accuracy of the U-Net with T1 images for glioma segmentation

Figure 4 presents examples of different MRI image weights and corresponding masks. Figure 5 illustrates some data augmentation results with the eADC map image.

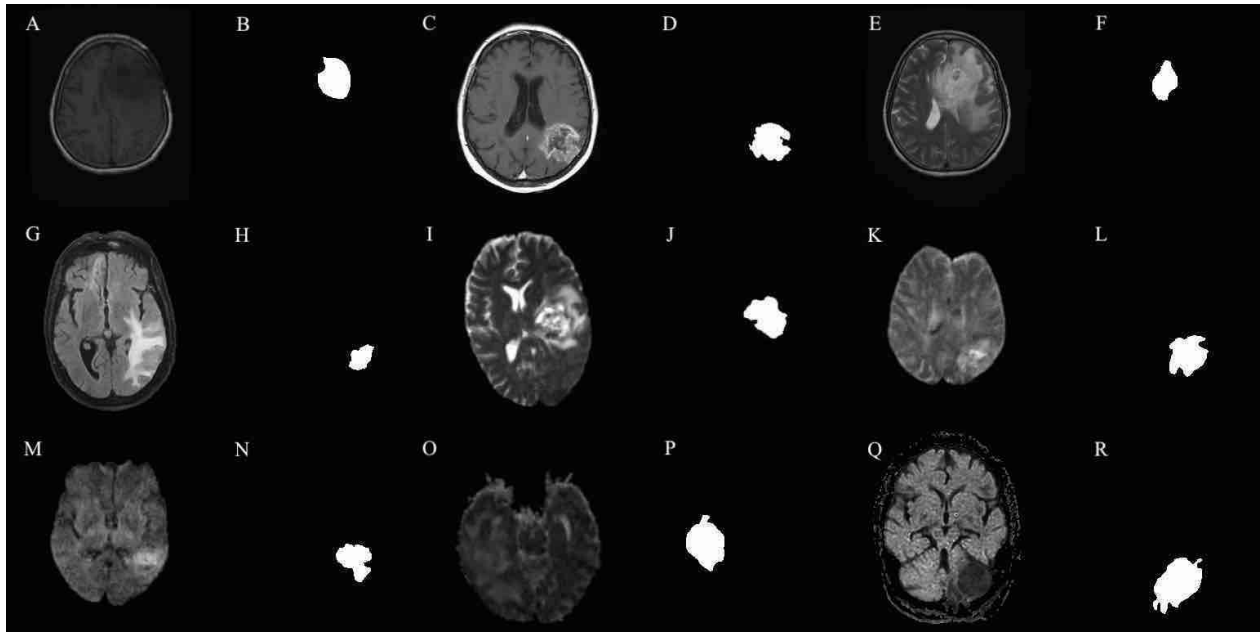


Figure 4- different MRI image weights and masks as U-Net input images. A-T1 weighted image. B-T1 mask. C-T1Gd weighted image. D-T1Gd mask. E-T2 weighted image. F-T2 mask. G- T2-FLAIR weighted image. H-T2-FLAIR mask I-DWI(b50) weighted image. J- DWI(b50) mask. K- DWI(b500) weighted image. L- DWI(b500) mask. M- DWI(b1000) weighted image. N- DWI(b1000) mask. O- ADC map image. P- ADC map mask. Q- eADC map image. R- eADC map mask.

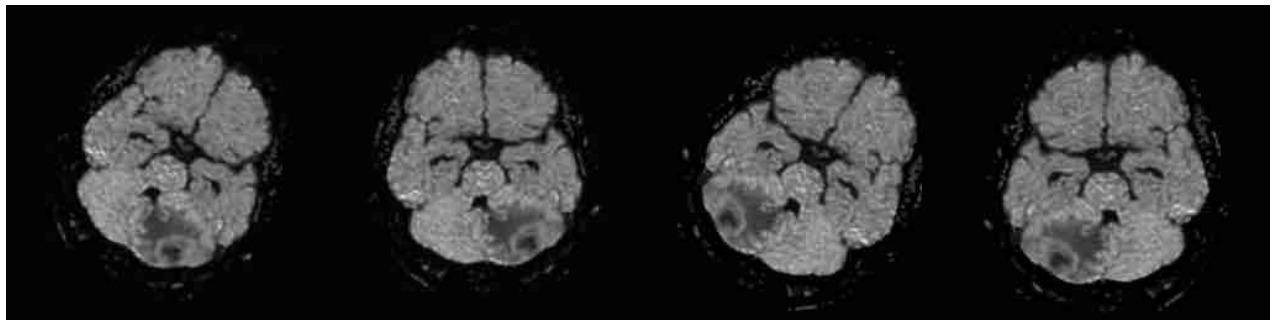


Figure 5- Data Augmentation technique examples of eADC maps

The segmented images obtained from U-Net with different MRI image-weighted as the input image are shown in figure 6.

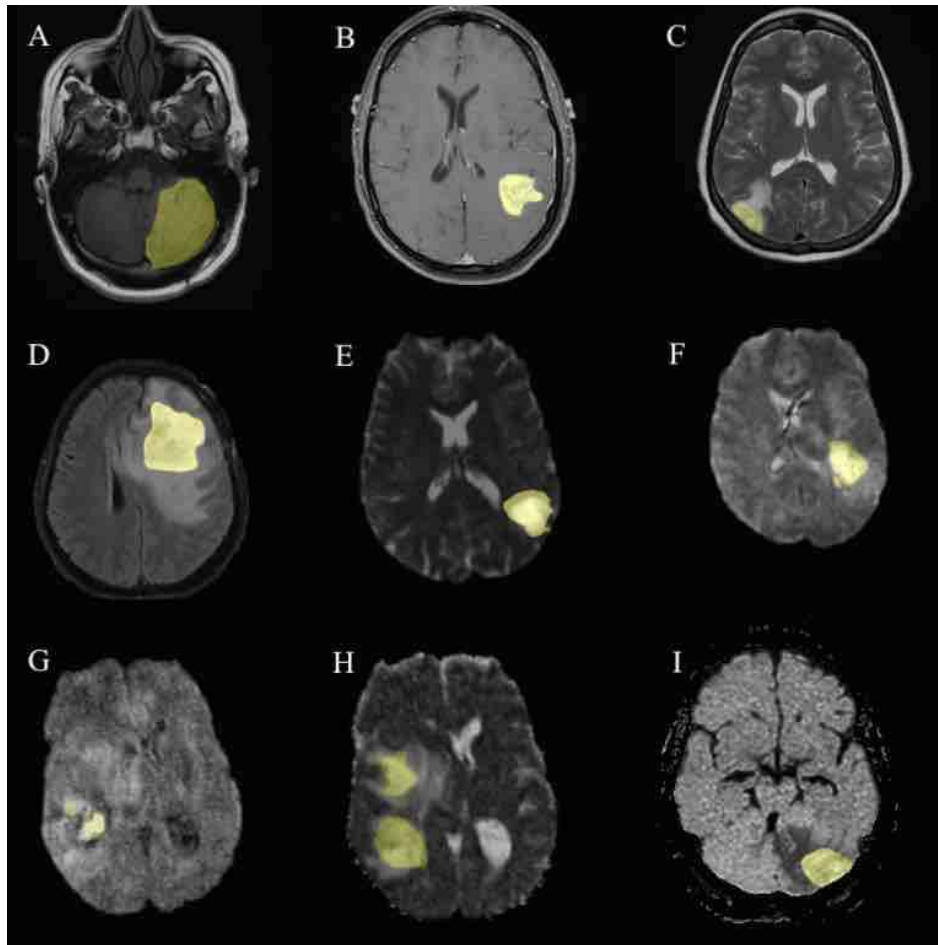


Figure 6- U-Net segmented output with different MRI image weights. A-T₁ B-T₁Gd C-T₂ D-T₂-FLAIR E-b50 F-b500 G-b1000 H-ADC map I-eADC map

Table 2 provides an overview of average accuracy, average Dice coefficient, and running time of one epoch of U-Net for each MRI image-weights.

Table 2- Dice coefficient, accuracy, and running time of the U-Net with different MRI image-weights for glioma segmentation

MRI image-weights	Average of Dice coefficient	Accuracy %	One epoch running time (s) ± standard deviation
T ₁	0.721	97.8	825.41±1.54
T ₁ Gd	0.694	97.6	841.43±1.98
T ₂	0.762	97.8	825.42±2.06
T ₂ FLAIR	0.896	96.9	839.42±1.23
DWI-b50	0.892	96.9	844.23±2.67
DWI-b500	0.872	96.8	843.43±2.04
DWI-b1000	0.752	96.8	828.42±1.95
ADC map	0.931	98.1	834.51±0.91
eADC map	0.944	98.9	825.42±1.02

4. Discussion

Glioma is the primary malignancy in brain tumors. Glioma tumor segmentation is a very important process for treatment decision programs. Traditionally, tumor segmentation has always been done by a radiologist. However, glioma segmentation has become a time-consuming process for radiologists. In recent years there has been growing interest in automatic brain segmentation. Much work on the potential of deep learning and machine learning has been carried out as an automatic segmentation for brain tumor segmentation [26], [28], [29]. The present study was designed to determine the effect of different MRI image-weights as the input image of U-Net on the accuracy of segmentation.

The normalization step applied in this work is efficient in terms of computational cost compared to the other normalization approaches such as [39], [46]. In this study, data Augmentation techniques were used to increase the number of U-Net image inputs and the accuracy of the U-Net. Loss functions have a critical role in deep networks. To obtain high performance from CNN-based architectures, hybrid loss functions have been proposed in several works [47]–[49]. We used the default loss function (i.e., cross-entropy) because of its low computational cost and efficiency with our images. The optimizer and activation function should be chosen carefully in deep network architectures. Although different optimizations (e.g., Lagrangian optimization [50]) and activation functions [51]–[53] have been applied in different works, we applied the sigmoid and ReLU activations and Adam optimizer on account of their efficiency in the proposed architecture with our datasets.

The most remarkable result from the data is that the accuracy and Dice coefficient of U-Net of different MRI image-weights are different. A possible explanation for these results may be related to U-Net input images.

Different MRI imaging protocols provided image weights with different information and contrast [33]–[35]. In summary, in this paper, we have used three different MRI imaging protocols as input images of U-Net: anatomical image-weights (T_1 , T_2 , T_2 FLAIR), diffusion-weighted imaging DWI (b50, b500, b1000, ADC map, eADC map), and post-contrast enhancement images (T_1 Gd). Conventional anatomic image weights will provide information about the anatomy of structure [33]. The contrast of T_1 , T_2 , and T_2 FLAIR image-weights mainly depends on the tissues' relaxation time [54]. DWI image contrast is based on the differences in Brownian motion of water molecules inside the tissue [35]. In DWI image-weights, the b-value is a factor that reflects the strength of the gradients used to generate DWI images [55], [56]. The higher the b-value, the stronger the diffusion effects on the image [55]. ADC map represents the diffusion coefficient of each pixel of the image. ADC reflects not only true diffusion but depends on microscopic perfusion, bulk tissue motion, and spatial orientation. An alternative to ADC maps, the exponential ADC (eADC) removes the T_2 shine-through artifact from the ADC map [57]. In recent years there has been growing interest in using different MRI image-weights for brain tumor detection and classification [58]–[61]. Many attempts have been made [37], [38], [62] with the purpose of DWI image-weights usage for brain tumor detection.

The most interesting finding was that U-Net with DWI image-weighted as the input image has higher glioma segmentation performance. A possible explanation for these results might be related to DWI image contrast and Brownian motion of water molecules. These results match those observed in earlier studies [36], [63]. Another critical finding after evaluating each DWI image-weights performance was that the ADC map and eADC map achieve higher results for glioma segmentation by U-Net. It seems possible that these results are due to the nature of eADC maps. ADC and eADC show us physiological information and diffusion coefficient data. The ADC map's signal intensity is related to tissue diffusion and T2 properties. Some tissue and abnormalities have prolonged T₂ relaxation time values that spill over into the ADC map, a phenomenon known as the T₂ shine-through artifact. T₂ shine-through artifact was removed in the eADC map. This factor may explain the higher U-Net performance on the eADC map rather than the ADC map for glioma segmentation. It is important to note that, as far as we know, this is the first study to use the eADC map for glioma segmentation by U-Net.

The results of this study show that T₁Gd image-weights have low performance for glioma segmentation by U-Net. A reasonable explanation for this result may be attributed to the glioma grade. Glioma border enhancement in T₁ post-contrast images was seen in high-grade glioma, and low-grade gliomas are rarely enhanced [64]. This discrepancy could be attributed to not enhancing and detecting glioma by U-Net in T₁Gd image-weights in the case of low-grade glioma. Our results have some similarities with Pouratian et al. I. [64] findings.

In this study, U-Net's T₂FLAIR performance for glioma segmentation was found higher than T₁, T₂, and T₁Gd image weights. These results may seem to be due to the FLAIR sequence being similar to a T₂-weighted image, except that the TE and TR times are very long. By doing so, abnormalities remain bright, but normal CSF fluid is attenuated and made dark. This sequence is very sensitive to pathology and makes the differentiation between CSF and an abnormality much easier.

It is encouraging to compare the result of the current study with that found in other studies. Importantly, most previous studies used the BraTs data set as the input image of U-Net. Using the BraTs data set, we could access the T₁, T₁Gd, and FLAIR image weights of glioma tumors. According to table 3, our results in anatomical image-weights (T₁, T₂, T₂FLAIR) and post enhancement image-weights (T₁Gd) have many similarities with previous studies. The mean Dice coefficient values of U-Net trained with T₁, T₁Gd, T₂, and T₂FLAIR image-weights are typical of previous findings, which used BraTs data set and U-net (Table 3). These results offer crucial evidence for our U-Net results validation that our U-net, trained with conventional anatomical MRI image-weights, works appropriately according to the previous studies. This finding confirms our U-Net result validation. Also, two experts in neuroradiology visually check the U-Net segmentation results accuracy of our data set for result validation purposes and rate the protentional clinical values of U-Net prediction results. U-Net performance validation with the radiologist is widely available and has been used in previous studies such as [65]. All U-Net segmentation results are considered satisfactory in terms of clinical applicability.

Table 3- Quantitative results of brain tumor segmentation algorithms published recently

Authors, Years	The image data set or image weights	Network	Mean Dice coefficient
Cabezas et al. 1.,2018 [66]	BraTs 2018	3D U-Net	0.74
Sun et al. ,2019 [67]	BraTs 2018	U-Net	0.71
Mehta and tal ,2019 [68]	BraTs 2018	3D U-Net	0.78
Yang et al. 1.,2019 [69]	BraTs 2017	U-Net combined with ResNet	0.748
Baid et al.,2020 [44]	BraTs 2018+ patient	U-Net	0.75, 0.81
Yang et al. 1.,2020 [70]	BraTs 2018	Novel U-Net dilated convolution DCU-Net	0.83
Naser and Deen, 2020 [20]	T1-T1Gd-FLAIR	U-Net and Vgg16 transfer learning	0.84
Yogananda et al., 2020 [31]	BraTs 2018	U-Net	0.80
Yang et al. 1. ,2020 [21]	BraTs 2015	Improved U-Net Deeper ResU-Net	0.88

Although the average Dice coefficient and accuracy of U-Net prediction with T₁, T₁Gd, T₂, and T₂-FLAIR are in line with previous studies (Table 3), we cannot be exactly compared our results to other studies since we used our specific data sets. Nevertheless, it is crucial to bear in mind that the BraTs data sets, which were used in previous studies for glioma segmentation with U-Net architecture, consist of T₁, T₁Gd, T₂, and T₂-FLAIR MRI images of glioma tumors and in the current study, we also used T₁, T₁Gd, T₂, and T₂-FLAIR and U-Net architecture. Therefore, our results, especially U-Net performance with anatomical images, can be compared to the previous study (Table 3) to validate the U-Net performance in the study. Using ADC maps and eADC maps for glioma segmentation by U-Net shows a clear advantage over other MRI imaging protocols studied in the current study. Also, the utility of advanced MRI imaging protocols, such as ADC maps, and eADC maps, over U-Net architecture to improve glioma segmentation is thus demonstrated. Also, we believe that this is the first time that eADC maps were used for glioma segmentation by U-Net.

5. Conclusion

The results of this study support the idea that we can use advanced MRI image weights for glioma segmentation by U-Net with higher performance. The best of our knowledge, no other authors have found that the eADC map as the input image of U-Net has high performance rather than other DWI imaging protocols (b50, b500, b1000, ADC map), conventional anatomical imaging protocols (T₁, T₂, T₂FLAIR), and T₁ post enhancement (T₁Gd) image-weights. This paper has highlighted the importance of input image information for U-Net training on the U-net performance on glioma segmentation. Our work has some limitations. Further data collection would be needed to create the big data set for U-Net training and achieve high accuracy for the training phase. Despite this, we believe our work could be a framework for using advanced MRI

imaging protocols with U-Net for glioma segmentation and classification. This approach has the potential to use other advanced MRI imaging protocols such as susceptibility-weighted imaging (SWI), dynamic contrast enhancement (DCE) imaging, arterial spin labeling (ASL), susceptibility contrast enhancement (SCE), diffusion tractography imaging (DTI), etc. for glioma segmentation and classification by U-Net. Also, as an extension of this work, the performance of the proposed approach can be compared with the performance of a capsule network since capsule networks can preserve spatial relationships of learned features and have been proposed recently for medical image classifications [71]–[73].

Data Availability

The datasets used and analyzed during the current study are available from the corresponding author on reasonable request.

Conflicts of Interest

The authors declare that they have no conflict of interests

Funding Statement

This study was supported by Isfahan University of Medical Sciences, Isfahan, I.R. Iran (grant number 399077).

Acknowledgment

The authors thank the Isfahan University of Medical Sciences for the financial support of this work.

Reference

- [1] A. N. Mamelak and D. B. Jacoby, “Targeted delivery of antitumoral therapy to glioma and other malignancies with synthetic chlorotoxin (TM-601),” *Expert Opin. Drug Deliv.*, vol. 4, no. 2, pp. 175–186, 2007.
- [2] M. L. Goodenberger and R. B. Jenkins, “Genetics of adult glioma,” *Cancer Genet.*, vol. 205, no. 12, pp. 613–621, 2012.
- [3] D. N. Louis *et al.*, “The 2021 WHO classification of tumors of the central nervous system: a summary,” *Neuro. Oncol.*, vol. 23, no. 8, pp. 1231–1251, 2021.
- [4] G. Mohan and M. M. Subashini, “Medical imaging with intelligent systems: a review,” *Deep Learn. parallel Comput. Environ. Bioeng. Syst.*, pp. 53–73, 2019.
- [5] S. C. Thust *et al.*, “Glioma imaging in Europe: a survey of 220 centres and

- recommendations for best clinical practice,” *Eur. Radiol.*, vol. 28, no. 8, pp. 3306–3317, 2018.
- [6] Q. Li *et al.*, “Glioma segmentation with a unified algorithm in multimodal MRI images,” *IEEE Access*, vol. 6, pp. 9543–9553, 2018.
- [7] M. Huang, W. Yang, Y. Wu, J. Jiang, W. Chen, and Q. Feng, “Brain tumor segmentation based on local independent projection-based classification,” *IEEE Trans. Biomed. Eng.*, vol. 61, no. 10, pp. 2633–2645, 2014.
- [8] S. Pereira, A. Pinto, V. Alves, and C. A. Silva, “Brain tumor segmentation using convolutional neural networks in MRI images,” *IEEE Trans. Med. Imaging*, vol. 35, no. 5, pp. 1240–1251, 2016.
- [9] R. Ranjbarzadeh, A. B. Kasgari, S. J. Ghoushchi, S. Anari, M. Naseri, and M. Bendeche, “Brain tumor segmentation based on deep learning and an attention mechanism using MRI multi-modalities brain images,” *Sci. Rep.*, vol. 11, no. 1, pp. 1–17, 2021.
- [10] G. M. Conte *et al.*, “Generative adversarial networks to synthesize missing T1 and FLAIR MRI sequences for use in a multisequence brain tumor segmentation model,” *Radiology*, vol. 299, no. 2, pp. 313–323, 2021.
- [11] Á. Györfi, L. Szilágyi, and L. Kovács, “A Fully Automatic Procedure for Brain Tumor Segmentation from Multi-Spectral MRI Records Using Ensemble Learning and Atlas-Based Data Enhancement,” *Appl. Sci.*, vol. 11, no. 2, p. 564, 2021.
- [12] I. Abd El Kader, G. Xu, Z. Shuai, S. Saminu, I. Javaid, and I. Salim Ahmad, “Differential deep convolutional neural network model for brain tumor classification,” *Brain Sci.*, vol. 11, no. 3, p. 352, 2021.
- [13] H. Chen, Z. Qin, Y. Ding, L. Tian, and Z. Qin, “Brain tumor segmentation with deep convolutional symmetric neural network,” *Neurocomputing*, vol. 392, pp. 305–313, 2020.
- [14] J. Amin, M. Sharif, M. Yasmin, and S. L. Fernandes, “Big data analysis for brain tumor detection: Deep convolutional neural networks,” *Futur. Gener. Comput. Syst.*, vol. 87, pp. 290–297, 2018.
- [15] H. Dong, G. Yang, F. Liu, Y. Mo, and Y. Guo, “Automatic brain tumor detection and segmentation using U-Net based fully convolutional networks,” in *annual conference on medical image understanding and analysis*, 2017, pp. 506–517.
- [16] A. Kermi, I. Mahmoudi, and M. T. Khadir, “Deep convolutional neural networks using U-Net for automatic brain tumor segmentation in multimodal MRI volumes,” in *International MICCAI Brainlesion Workshop*, 2018, pp. 37–48.
- [17] W. Wu *et al.*, “An intelligent diagnosis method of brain MRI tumor segmentation using deep convolutional neural network and SVM algorithm,” *Comput. Math. Methods Med.*, vol. 2020, 2020.
- [18] Y. Bhanothu, A. Kamalakannan, and G. Rajamanickam, “Detection and classification of brain tumor in MRI images using deep convolutional network,” in *2020 6th International*

- Conference on Advanced Computing and Communication Systems (ICACCS)*, 2020, pp. 248–252.
- [19] Z. Zhou, Z. He, and Y. Jia, “AFPNet: A 3D fully convolutional neural network with atrous-convolution feature pyramid for brain tumor segmentation via MRI images,” *Neurocomputing*, vol. 402, pp. 235–244, 2020.
- [20] M. A. Naser and M. J. Deen, “Brain tumor segmentation and grading of lower-grade glioma using deep learning in MRI images,” *Comput. Biol. Med.*, vol. 121, p. 103758, 2020.
- [21] T. Yang, J. Song, L. Li, and Q. Tang, “Improving brain tumor segmentation on MRI based on the deep U-net and residual units,” *J. Xray. Sci. Technol.*, vol. 28, no. 1, pp. 95–110, 2020.
- [22] C. Vijayakumar, G. Damayanti, R. Pant, and C. M. Sreedhar, “Segmentation and grading of brain tumors on apparent diffusion coefficient images using self-organizing maps,” *Comput. Med. Imaging Graph.*, vol. 31, no. 7, pp. 473–484, 2007.
- [23] A. A. Pravitasari *et al.*, “UNet-VGG16 with transfer learning for MRI-based brain tumor segmentation,” *Telkomnika*, vol. 18, no. 3, pp. 1310–1318, 2020.
- [24] T. Henry *et al.*, “Top 10 BraTS 2020 challenge solution: Brain tumor segmentation with self-ensembled, deeply-supervised 3D-Unet like neural networks,” *arXiv e-prints*, p. arXiv-2011, 2020.
- [25] T. Sadad *et al.*, “Brain tumor detection and multi-classification using advanced deep learning techniques,” *Microsc. Res. Tech.*, vol. 84, no. 6, pp. 1296–1308, 2021.
- [26] K. Kaewrak, J. Soraghan, G. Di Caterina, and D. Grose, “TwoPath U-Net for automatic brain tumor segmentation from multimodal MRI data,” in *International MICCAI Brainlesion Workshop*, 2020, pp. 300–309.
- [27] K. Thiruvankadam and K. Nagarajan, “Fully automatic brain tumor extraction and tissue segmentation from multimodal MRI brain images,” *Int. J. Imaging Syst. Technol.*, vol. 31, no. 1, pp. 336–350, 2021.
- [28] X. Zhao, Y. Wu, G. Song, Z. Li, Y. Zhang, and Y. Fan, “A deep learning model integrating FCNNs and CRFs for brain tumor segmentation,” *Med. Image Anal.*, vol. 43, pp. 98–111, 2018.
- [29] F. Isensee, P. F. Jäger, P. M. Full, P. Vollmuth, and K. H. Maier-Hein, “Nnu-net for brain tumor segmentation,” in *International MICCAI Brainlesion Workshop*, 2020, pp. 118–132.
- [30] L. Fidon, S. Ourselin, and T. Vercauteren, “Generalized Wasserstein Dice Score, Distributionally Robust Deep Learning, and Ranger for brain tumor segmentation: BraTS 2020 challenge,” *arXiv Prepr. arXiv2011.01614*, 2020.
- [31] C. G. B. Yogananda *et al.*, “A Fully automated deep learning network for brain tumor segmentation,” *Tomography*, vol. 6, no. 2, pp. 186–193, 2020.

- [32] R. A. Zeineldin, M. E. Karar, J. Coburger, C. R. Wirtz, and O. Burgert, “DeepSeg: deep neural network framework for automatic brain tumor segmentation using magnetic resonance FLAIR images,” *Int. J. Comput. Assist. Radiol. Surg.*, vol. 15, no. 6, pp. 909–920, 2020.
- [33] F. Lüsebrink, A. Sciarra, H. Mattern, R. Yakupov, and O. Speck, “T 1-weighted in vivo human whole brain MRI dataset with an ultrahigh isotropic resolution of 250 μm ,” *Sci. data*, vol. 4, no. 1, pp. 1–12, 2017.
- [34] L. Minati and W. P. Węglarz, “Physical foundations, models, and methods of diffusion magnetic resonance imaging of the brain: A review,” *Concepts Magn. Reson. Part A An Educ. J.*, vol. 30, no. 5, pp. 278–307, 2007.
- [35] P. W. Schaefer, P. E. Grant, and R. G. Gonzalez, “Diffusion-weighted MR imaging of the brain,” *Radiology*, vol. 217, no. 2, pp. 331–345, 2000.
- [36] J. Lee, S. H. Choi, J. Kim, C. Sohn, S. Lee, and J. Jeong, “Glioma grading using apparent diffusion coefficient map: application of histogram analysis based on automatic segmentation,” *NMR Biomed.*, vol. 27, no. 9, pp. 1046–1052, 2014.
- [37] R. Jiang *et al.*, “Diffusion kurtosis imaging can efficiently assess the glioma grade and cellular proliferation,” *Oncotarget*, vol. 6, no. 39, p. 42380, 2015.
- [38] R. K. Soliman, A. A. Essa, A. A. S. Elhakeem, S. A. Gamal, and M. M. A. Zaitoun, “Texture analysis of apparent diffusion coefficient (ADC) map for glioma grading: Analysis of whole tumoral and peri-tumoral tissue,” *Diagn. Interv. Imaging*, vol. 102, no. 5, pp. 287–295, 2021.
- [39] E. Goceri, “Fully automated and adaptive intensity normalization using statistical features for brain MR images,” *Celal Bayar Univ. J. Sci.*, vol. 14, no. 1, pp. 125–134, 2018.
- [40] J. C. Reinhold, B. E. Dewey, A. Carass, and J. L. Prince, “Evaluating the impact of intensity normalization on MR image synthesis,” in *Medical Imaging 2019: Image Processing*, 2019, vol. 10949, pp. 890–898.
- [41] Y.-D. Zhang *et al.*, “Image based fruit category classification by 13-layer deep convolutional neural network and data augmentation,” *Multimed. Tools Appl.*, vol. 78, no. 3, pp. 3613–3632, 2019.
- [42] E. Goceri, “Image augmentation for deep learning based lesion classification from skin images,” in *2020 IEEE 4th International Conference on Image Processing, Applications and Systems (IPAS)*, 2020, pp. 144–148.
- [43] A. Baratloo, M. Hosseini, A. Negida, and G. El Ashal, “Part 1: simple definition and calculation of accuracy, sensitivity and specificity,” 2015.
- [44] U. Baid *et al.*, “A novel approach for fully automatic intra-tumor segmentation with 3D U-Net architecture for gliomas,” *Front. Comput. Neurosci.*, vol. 14, p. 10, 2020.
- [45] F. Milletari, N. Navab, and S.-A. Ahmadi, “V-net: Fully convolutional neural networks for volumetric medical image segmentation,” in *2016 fourth international conference on 3D vision (3DV)*, 2016, pp. 565–571.

- [46] E. Goceri, “Intensity normalization in brain MR images using spatially varying distribution matching,” in *11th Int. Conf. on computer graphics, visualization, computer vision and image processing (CGVCVIP 2017)*, 2017, pp. 300–304.
- [47] Z. Li *et al.*, “Low-dose CT image denoising with improving WGAN and hybrid loss function,” *Comput. Math. Methods Med.*, vol. 2021, 2021.
- [48] E. GÖÇERİ, “An Application for Automated Diagnosis of Facial Dermatological Diseases,” *İzmir Katip Çelebi Üniversitesi Sağlık Bilim. Fakültesi Derg.*, vol. 6, no. 3, pp. 91–99, 2021.
- [49] E. Goceri, “Diagnosis of skin diseases in the era of deep learning and mobile technology,” *Comput. Biol. Med.*, vol. 134, p. 104458, 2021.
- [50] H. Kervadec, J. Dolz, J. Yuan, C. Desrosiers, E. Granger, and I. Ben Ayed, “Constrained deep networks: Lagrangian optimization via log-barrier extensions,” *arXiv Prepr. arXiv1904.04205*, 2019.
- [51] E. Goceri, “Skin disease diagnosis from photographs using deep learning,” in *ECCOMAS thematic conference on computational vision and medical image processing*, 2019, pp. 239–246.
- [52] J. Kisel’ák, Y. Lu, J. Švihra, P. Szépe, and M. Stehlík, “‘SPOCU’: scaled polynomial constant unit activation function,” *Neural Comput. Appl.*, vol. 33, no. 8, pp. 3385–3401, 2021.
- [53] E. Goceri, “Analysis of deep networks with residual blocks and different activation functions: classification of skin diseases,” in *2019 Ninth international conference on image processing theory, tools and applications (IPTA)*, 2019, pp. 1–6.
- [54] J. Z. Bojorquez, S. Bricq, C. Acquitter, F. Brunotte, P. M. Walker, and A. Lalande, “What are normal relaxation times of tissues at 3 T?,” *Magn. Reson. Imaging*, vol. 35, pp. 69–80, 2017.
- [55] J. H. Burdette, D. D. Durden, A. D. Elster, and Y.-F. Yen, “High b-value diffusion-weighted MRI of normal brain,” *J. Comput. Assist. Tomogr.*, vol. 25, no. 4, pp. 515–519, 2001.
- [56] P. B. Kingsley and W. G. Monahan, “Selection of the optimum b factor for diffusion-weighted magnetic resonance imaging assessment of ischemic stroke,” *Magn. Reson. Med. An Off. J. Int. Soc. Magn. Reson. Med.*, vol. 51, no. 5, pp. 996–1001, 2004.
- [57] J. M. Provenzale, S. T. Engelter, J. R. Petrella, J. S. Smith, and J. R. MacFall, “Use of MR exponential diffusion-weighted images to eradicate T2" shine-through" effect.,” *AJR. Am. J. Roentgenol.*, vol. 172, no. 2, pp. 537–539, 1999.
- [58] Y. Bliesener, R. M. Lebel, J. Acharya, R. Frayne, and K. S. Nayak, “Pseudo Test-Retest Evaluation of Millimeter-Resolution Whole-Brain Dynamic Contrast-enhanced MRI in Patients with High-Grade Glioma,” *Radiology*, p. 203628, 2021.
- [59] A. Y. Lakshmi, V. V. R. Chandra, M. S. MCH, and M. D. Rukmangada, “Utility of Perfusion Weighted MRI and MR Spectroscopy in Intra Cerebral Glioma Grading.”

- [60] A. Vamvakas *et al.*, “Imaging biomarker analysis of advanced multiparametric MRI for glioma grading,” *Phys. Medica*, vol. 60, pp. 188–198, 2019.
- [61] X. Li *et al.*, “Glioma grading by microvascular permeability parameters derived from dynamic contrast-enhanced MRI and intratumoral susceptibility signal on susceptibility weighted imaging,” *Cancer Imaging*, vol. 15, no. 1, pp. 1–9, 2015.
- [62] H. S. Choi, A. H. Kim, S. S. Ahn, N. Shin, J. Kim, and S.-K. Lee, “Glioma grading capability: comparisons among parameters from dynamic contrast-enhanced MRI and ADC value on DWI,” *Korean J. Radiol.*, vol. 14, no. 3, pp. 487–492, 2013.
- [63] D. Simon *et al.*, “Diffusion-weighted imaging-based probabilistic segmentation of high- and low-proliferative areas in high-grade gliomas,” *Cancer Imaging*, vol. 12, no. 1, p. 89, 2012.
- [64] N. Pouratian, A. Asthagiri, J. Jagannathan, M. E. Shaffrey, and D. Schiff, “Surgery Insight: the role of surgery in the management of low-grade gliomas,” *Nat. Clin. Pract. Neurol.*, vol. 3, no. 11, pp. 628–639, 2007.
- [65] Y. Zhang *et al.*, “Brain Tumor Segmentation From Multi-Modal MR Images via Ensembling UNets,” *Front. Radiol.*, vol. 1, 2021.
- [66] M. Cabezas *et al.*, “Survival prediction using ensemble tumor segmentation and transfer learning,” *arXiv Prepr. arXiv1810.04274*, 2018.
- [67] L. Sun, S. Zhang, H. Chen, and L. Luo, “Brain tumor segmentation and survival prediction using multimodal MRI scans with deep learning,” *Front. Neurosci.*, vol. 13, p. 810, 2019.
- [68] R. Mehta and T. Arbel, “3D U-Net for brain tumour segmentation,” in *International MICCAI Brainlesion Workshop*, 2018, pp. 254–266.
- [69] C. Yang *et al.*, “Automatic brain tumor segmentation method based on modified convolutional neural network,” in *2019 41st Annual International Conference of the IEEE Engineering in Medicine and Biology Society (EMBC)*, 2019, pp. 998–1001.
- [70] T. Yang, Y. Zhou, L. Li, and C. Zhu, “DCU-Net: Multi-scale U-Net for brain tumor segmentation,” *J. Xray. Sci. Technol.*, vol. 28, no. 4, pp. 709–726, 2020.
- [71] E. Goceri, “CapsNet topology to classify tumours from brain images and comparative evaluation,” *IET Image Process.*, vol. 14, no. 5, pp. 882–889, 2020.
- [72] E. Goceri, “Analysis of capsule networks for image classification,” in *International Conference on Computer Graphics, Visualization, Computer Vision and Image Processing*, 2021.
- [73] E. Goceri, “Capsule neural networks in classification of skin lesions,” in *International Conference on Computer Graphics, Visualization, Computer Vision and Image Processing*, 2021, pp. 29–36.